Applied Materials Today 27 (2022) 101442

Contents lists available at ScienceDirect

Applied Materials Today

journal homepage: www.elsevier.com/locate/apmt

# Biomimetic macroporous hydrogel with a triple-network structure for full-thickness skin regeneration

Xiaojun Long[a,b,1], Xiao Xu[a,1], Deshun Sun[a,1], Yi Hong[b], Caining Wen[a], Yixin Xie[a], Bing Yan[a], Huawei Zhang[c], Qi Ge[d], Wencui Li[a,*], Li Duan[a,*], Hongwei Ouyang[b,*], Daping Wang[a,c,*]

[a] Shenzhen Second People's Hospital, First Affiliated Hospital of Shenzhen University Health Science Center, Shenzhen 518035, China
[b] Dr. Li Dak Sum and Yip Yio Chin Center for Stem Cells and Regenerative Medicine, Zhejiang University School of Medicine, Hangzhou 310003, China
[c] Department of Biomedical Engineering, Southern University of Science and Technology, Shenzhen, 518055, China
[d] Department of Mechanical and Energy Engineering, Southern University of Science and Technology, Shenzhen 518055, China

ARTICLE INFO

*Article history:*
Received 3 December 2021
Revised 24 February 2022
Accepted 7 March 2022

ABSTRACT

Full-thickness skin repair is still a challenge in clinical practice because it is extremely difficult for dermal reconstruction and calls for a promising strategy to achieve quick sutureless closure and high-quality dermal restoration for large acute skin defects. Inspired by the unique composition, mechanical properties and microscopic architecture of skin tissue, a novel biomimetic hydrogel with a triple-network structure that mimics the extracellular matrix (ECM) composition has been reported. A composite biomimetic hydrogel was prepared using ECM-derived biopolymers, gelatin methacryloyl (GelMA) and N-(2-aminoethyl)-4-(4-(hydroxymethyl)-2–methoxy-5-nitro-sophenoxy) butanamide (NB)-linked sodium alginate (Alg-NB) and the photoinitiator lithium phenyl-2,4,6-trimethylbenzoylphosphinate (LAP). This biomimetic hydrogel can undergo rapid gelling under UV irradiation (approximately 3 s), has strong mechanical properties (mechanical strength ≈530 kPa) with UV-ionic-crosslinking, and shows strong adhesion to wet tissue. In vitro two-dimensional culture of human skin fibroblasts (HSFs) confirmed that the biomimetic hydrogel has excellent biocompatibility, and HSFs on the surface grow into cell clusters because of the macroporous structures of the hydrogel (pore diameter ≈160 $\mu$m). The subcutaneous implantation of the biomimetic hydrogel in Sprague-Dawley (SD) rats confirmed its biocompatibility and low biodegradation in vivo. Moreover, in an SD rat full-thickness skin defect model, this engineered biomimetic hydrogel not only could be used for sutureless wound closure strategies but also could accelerate the reconstitution of dermal tissue with skin appendages. This study provides an effective strategy of quick sutureless wound closure and highly efficient repair for full-thickness skin defects and shows enormous potential for tissue regeneration in clinical applications.



## 1. Introduction

Full-thickness skin defects are the most common injury in daily life, war and disaster [1,2] and have a serious influence on the quality of life of patients [3,4]. Restriction to the limited self-repair ability of skin, especially for the dermal construction of full-thickness dermal skin defects, is very difficult [5,6]. Engineered autologous dermal substitutes such as tissue-engineered skin (mostly created by expanding skin cells) [7], acellular dermal matrix [8], and biomaterial scaffolds [9,10] have emerged as promising alternative approaches to repair damaged tissues. Among them, biomaterial scaffolds have the advantages of widespread sources, moderate prices, simple preparation and adjustable physical/chemical properties, showing great potential for skin barriers, angiogenesis, wound healing, and skin reconstruction applications.

Recently, hydrogels, especially biomimetic hydrogels, which contain the main extracellular matrix (ECM)-derived component of skin, can function as scaffolds with three-dimensional (3D) networks and have been proven to show great potential in the field of full-thickness skin repair [11–13]. Generally, biomimetic hydrogels are formed with biopolymers, which play an important role in the process of biological signals and cell adhesion and can be degraded and reconstructed by cells as matrix materials, such as collagen [14], protein (such as gelatin) [15], hyaluronic acid (HA), alginate (Alg) [16], heparin [17], chitosan [18], and chondroitin sulfate [19]. However, most biomimetic hydrogels have the drawbacks of low adhesion to wet tissues [20–22] and poor mechanical properties

* Corresponding authors.
*E-mail addresses:* 13923750767@163.com (W. Li), duanl@szu.edu.cn (L. Duan), hwoy@zju.edu.cn (H. Ouyang), dapingwang1963@qq.com (D. Wang).
[1] These authors contributed equally to this work

https://doi.org/10.1016/j.apmt.2022.101442
2352-9407/

[23,24], which make them unable to be well adapted to dynamic wounds with frequency movement and may lead to potential immunogenic reactions, resulting in unsatisfactory wound healing effects [25,26].

To improve the wet tissue adhesive ability of hydrogels, the strategy of grafting modification with small molecules have been proved to be anticipated. For example, Guo et al. constructed an series of adhesive hydrogels based on HA-graft-dopamine and reduced graphene oxide (rGO), the adhesion mechanism can be contributed to the imide formation or Michael-type reaction of catechol and quinone groups on rGO@PDA with amino or thiol groups on the protein, the hydrogels are an excellent wound dressing for full-thickness skin repair [27]. However, the potential cytotoxicity for rGO made it cannot become the best candidate to improve the adhesive ability of hydrogels. In our previous work, we constructed a strongly adhesive hemostatic hydrogel based on a double-network hydrogel with a UV-responsive *N*-(2-aminoethyl)−4-(4-(hydroxymethyl)−2–methoxy-5-nitrosophe-noxy) butanamide (NB) grafted with HA (HA-NB) and a methacrylate anhydride-grafted gelatin (GelMA). Under UV irradiation, the hydroxyl methyl on the NB becomes an aldehyde group. This property enables the "molecular glue" to bond with the surface of wet tissue through a Schiff base reaction, showing good adhesion to wet tissue [28]. However, the mechanical properties of the hydrogel need to be improved, especially when the concentration of matrix material is low (approximately 5 wt%), and various researches had proved that lower concentrations of GelMA could be more suitable for cell proliferation [29,30], and soft tissues regeneration [4]. Instead of the strategy of increasing the concentration of the hydrogels, many works have found that ionic crosslinking can greatly improve the mechanical properties of hydrogels. For example, Sheikhi et al. used GelMA and methacrylate-modified alginate (AlgMA) as the matrix material to greatly improve the mechanical properties of hydrogels by introducing ionic crosslinking [31]. However, this hydrogel lacks sufficient chemical binding anchor points with tissue, and its tissue adhesion ability is not ideal.

In addition, it was reported that injectable 3D hydrogel scaffolds with macroporous structures could facilitate cell migration, resulting in rapid cutaneous tissue regeneration and tissue structure formation [32,33]. The macroporous structure provides cells a 3D organization, allows the supply of nutrients, and allows removal of waste metabolites; most importantly, they also provide large, interconnected pores that facilitate blood vessel in-growth [34,35]. However, the pore size of the porous structure of most injectable hydrogels was less than 100 $\mu$m, and the increase in hydrogel concentration and higher crosslinking density might result in a reduction in pore size [36,37]. Although developed 3D printing strategies could be used to build a microstructure with macroporous (pores with a diameter larger than 100 $\mu$m), the preparation process for 3D printing is complicated, and most printed hydrogels can be used only as implants [38,39]. Therefore, the development of injectable biomimetic hydrogel with strong tissue adhesion, super mechanical properties, and macroporous microstructure properties as a wound dressing is still highly anticipated.

Inspired by the facts above, we envisioned fabricating a triple-dynamic-bond cross-linked adhesive hydrogels by rationally engineering the functional building blocks to endow the hydrogels with injectability, rapid gelling, strong adjustable mechanical, and macroporous microstructure properties, which could efficiently sutureless wound closure and promote wound closure. Herein, a novel ECM-derived biopolymers GelMA/Alg-NB/LAP, with three-network was constructed. Gelatin and Alg (fibrous protein and stromal analog in dermal dermis) were grafted and modified as GelMA (Fig. S1a) and Alg-NB (Fig. S1b), respectively, and hydrogel was formed with a triple-network through UV crosslinking and ionic crosslinking (Fig. 1a). MA is UV responsive, and acrylamide bonds can be synthesized by lithium phenyl-2,4,6-trimethylbenzoylphosphinate (LAP) initiator induction and UV irradiation (forming the first network, Fig. 1b). UV-sensitive small-molecule NB was selected to graft Alg to obtain Alg-NB. UV light-generated aldehyde groups on NB can react with GelMA and $NH_2$ groups in the tissue in the Schiff base (forming the second network, Fig. 1a, b). Furthermore, calcium ion crosslinking forms a triple-network structure (Fig. 1b). The characteristics of the UV photogenic aldehyde group on NB can improve the tissue adhesive ability of the hydrogel, and the triple-network construct can achieve excellent mechanical properties. Surprisingly, the addition of ionic crosslinking resulted in a microporous architecture. Then, the biocompatibility and biodegradation of the hydrogels *in vitro* and *in vivo* were investigated. Finally, a full-thickness skin defect model of SD rats was constructed, supplemented with the injectable hydrogel, which was then integrated into the full-thickness skin defect by UV crosslinking and ion crosslinking in situ. The integration effect of hydrogel and surrounding tissues was analyzed, and the effect and mechanism of wound repair were evaluated.

## 2. Method and materials

### 2.1. Synthesis of methylacrylated gelatin

GelMA (Fig. S1a) was purchased from Haining Jurassic Biotechnology Co., Ltd., and the synthesis process had described previously [28,40]. Briefly, type A gelatin (Sigma-Aldrich) was dissolved in PBS to make a 10% w/v homogeneous solution. Then a 0.1 mL methacrylic anhydride (MA) (Sigma-Aldrich) per gram of gelatin was added to the gelatin solution with continuous stirring. The mixture was allowed to react to form GelMA. Then, the GelMA solution was dialyzed against deionized water, frozen overnight, lyophilized and stored at − 20 °C until further use.

### 2.2. Preparation of Alg-NB

As shown in Fig. S1b, first, Alg (1 g, Aladdin Chemical Reagent, molecular weights (Mw) is about 20,000–50,000, M/G units is about 1:2) was dissolved in 2-(N-morphine) ethanesulfonic acid hydrate (MES, 0.01 mol/L, 100 mL; pH=5.3 (Aladdin Chemical Reagent)) buffer solution and reacted at 35 °C. After Alg was completely dissolved, 60 mg NB (Haining Jurassic Biotechnology Co., Ltd.) was dissolved in 10 mL of dimethyl sulfoxide (DMSO, Aladdin Chemical Reagent) and added to the reaction system. Then, 4-(4,6-dimethoxy-triazine-2-yl)−4-methylmoroline hydrochloride (DMTMM, 1.2 g, Aladdin Chemical Reagent) was added to the system three times, at an interval of 0.5∼1 h. After the last addition, the reaction was allowed to complete for 3 h. The whole process was completed under stirring. Finally, dialysis with 0.1 M NaCl solution (pH=3.5) for 2 days and then with deionized water for 2 days was performed, and Alg-NB was obtained after freeze drying. Alg-NB was sealed and preserved in darkness.

### 2.3. Preparation of hydrogel

GelMA and the prepared Alg-NB were mixed to prepare glue solutions with different composition ratios. In this work, the concentration of GelMA was set as 5 wt%; the polymerization initiator lithium phenyl-2,4,6-trimethylbenzoylphosphinate (LAP, 0.1 wt%, Haining Jurassic Biotechnology Co., Ltd.) was added to the mixture; the ratios of Alg-NB to GelMA were 1:10 (GelMA/Alg-NB1/LAP), 1:5 (GelMA/Alg-NB2/LAP), and 1:2.5 (GelMA/Alg-NB3/LAP); and ultraviolet light (UV) (365 nm, 30 mW/cm$^2$) was applied for UV crosslinking (to form the G-A-l hydrogel). Then, the mixture was soaked in $CaCl_2$ solution ($CaCl_2$:GelMA = 0.13) for calcium ion crosslinking (to form the G-A-ʟ-i hydrogel) (Fig. S4).

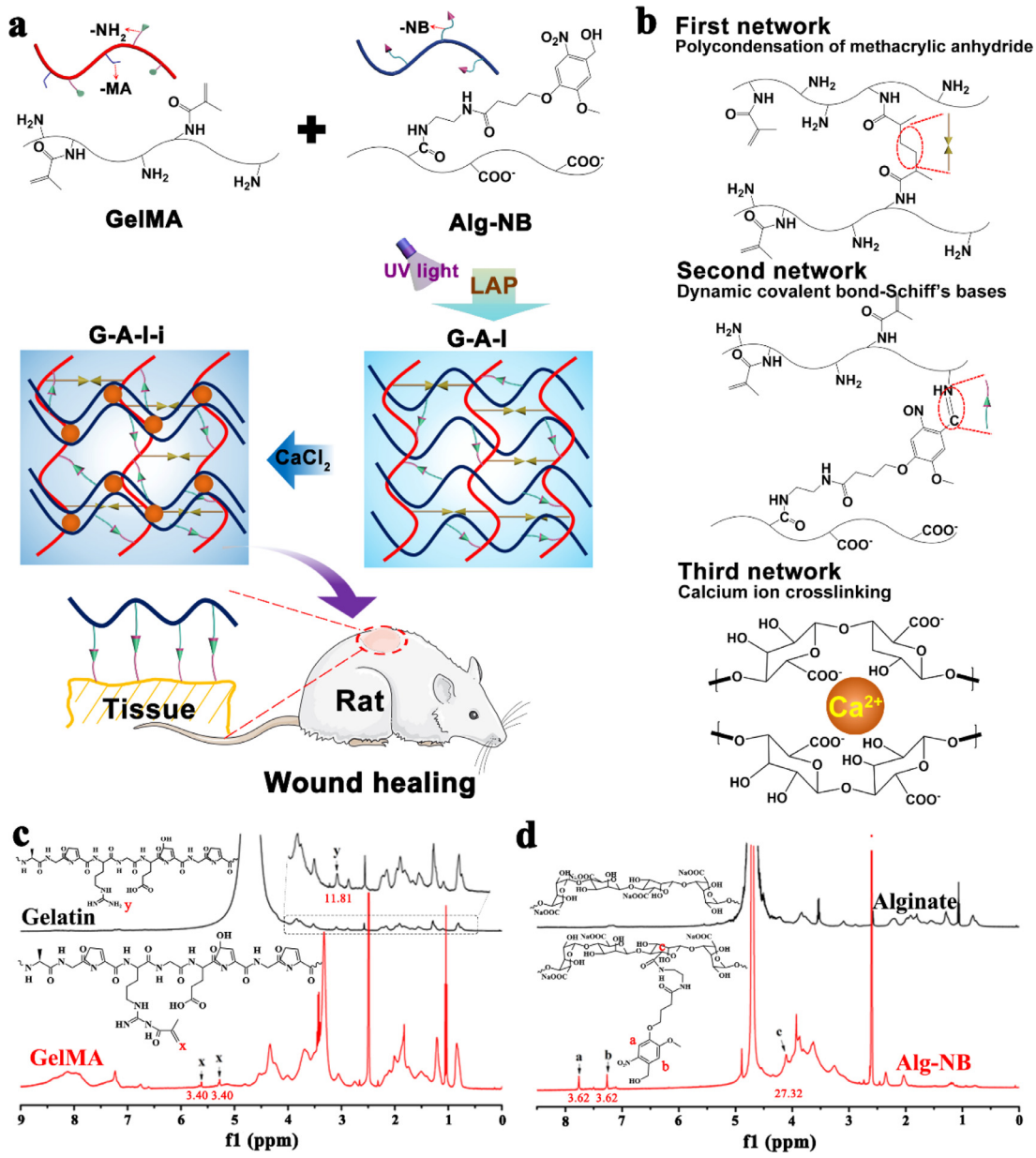


**Fig. 1.** UV-ionic-crosslinking (UIC) mechanism for three-network hydrogel and structure characterization of GelMA and Alg-NB. (a) Schematic illustration of UIC mechanism for hydrogel construction and full-thickness skin wound healing application; (b) Structural scheme of three-network formed for GelMA and Alg-NB, first network: polycondensation of methacrylic anhydride (GelMA/GelMA); second network: dynamic covalent bond-Schiff's bases (GelMA/Alg-NB); third network: calcium ion crosslinking (Alg-NB/Alg-NB); Structure characterization of GelMA (c) and Alg-NB (d) by $^1$H NMR (500 MHz), prepared in $D_2O$ at room temperature.

### 2.4. Characterization

The degree of methacrylation of gelatin for GelMA and nitrobenzyl group substitution for Alg-NB were determined using $^1$H-nuclear magnetic resonance ($^1$H NMR-500 M, Avance III 500 M with the Prodigy Platform, Switzerland). The gelatin, GelMA, alginate, and Alg-NB samples were prepared in $D_2O$ at room temperature, and the tested concentration of all the samples was approximately 8 mg/mL. The degree of methacrylation for GelMA [28] and the degree of NB substitution for Alg-NB [41] were calculated by integrating the peak areas of the results into the 1HNMR spectra (Fig. 1c, d).

$$\text{Degree of methacrylation (DM)} = \frac{I_x}{I_y} \times 100$$

$$\text{Degree of NB substitution (DN)} = \frac{I_a + I_b}{2I_c} \times 100$$

The rheological properties of various hydrogels were characterized using a photorheometer with parallel-plate (Discovery HR-3, TA, USA) geometry and an OmniCure Series 2000 (365 nm, 30 mW/cm$^2$) at 37 °C for the UV crosslinking of hydrogels. Tissue adhesion properties were determined by uniaxial tensile tests with an MTS uniaxial testing machine (Criterion model 43, MN, USA). Briefly, as shown in Fig. 3c, two 3.5 cm × 2.5 cm pig casings with good light transmission ability were attached to two glass slices with the help of cyanoacrylate glue, and hydrogels were formed in situ between them. The detached stress per unit area was used as a reference to evaluate the tissue adhesive strength of the tested hydrogels. The compressive stress–strain measurements were characterized using a tensile-compressive tester (Instron-5543 with a 1 kN sensor), and the hydrogels were prepared as a column structure for compression-crack tests (10 mm in diameter and 4 mm in height). The internal microstructure of hydrogels was characterized

by scanning electron microscopy (SEM) (Hitachi Model TM-1010, Japan). The swelling ratio (SR) of the hydrogel was calculated according to the equation below [36], in which $W_d$ is the dry weight after hydrogels were freeze dried; then, the freeze-dried hydrogels were incubated in PBS at 37 °C and weighed at certain time points ($W_s$).

$$SR = \frac{W_s - W_d}{W_d}$$

### 2.5. Cell culture

Human skin fibroblast cells (HSFs) were cultured on PS dishes in Dulbecco's modified Eagle's medium (DMEM; CellMax) supplemented with 10% fetal bovine serum (FBS, CellMax), 1% antibiotic solution containing 10,000 units/mL penicillin, and 10,000 mg/mL streptomycin (CellMax). After the cells were seeded on PS dishes, they were incubated in a humidified atmosphere with 5% $CO_2$ at 37 °C. The cultured cells were harvested with 0.25% trypsin/EDTA (CellMax) and suspended in fresh culture media for the next subculture experiments.

### 2.6. Cell viability

HSFs were selected to test the cell viability and cell proliferation of the hydrogels. First, GelMA, G-A-l, and G-A-L-i hydrogels were formed in situ in 24-well plates. Then, HSFs (20,000 cells/cm$^2$) were seeded on the surface of the GelMA, G-A-l, and G-A-L-i hydrogels and incubated in a humidified atmosphere with 5% $CO_2$ at 37 °C. After the cells were cultured for 1, 3 and 5 days, a live-dead cell staining kit (Abnova) was used to measure the cell viability of hydrogels based on the simultaneous determination of living and dead cells with two probes: calcein-AM for intracellular esterase activity and propidium iodide for plasma membrane integrity. The uptake of fluorescent indicators was detected using a confocal microscope, and cells cultured on the surface of PS substrate were used as a control group. After the cells were cultured for 1, 4 and 7 days, cell counting kit-8 (CCK-8, Dojingdo Laboratories, Kumamoto, Japan) solution was added to the wells at a concentration ratio of 1/10 with the culture solution. Then, the cells were incubated for 3 h in the incubator, and the OD value was measured at 450 nm with a microplate reader (Multiskan MK3). Briefly, Cell Counting Kit-8 (CCK-8, Dojingdo Laboratories, Kumamoto, Japan) solution was added to the wells at a concentration ratio of 1/10 with the culture solution and incubated for 3 h in the incubator. The OD value was measured at 450 nm with a microplate reader (Multiskan MK3).

### 2.7. In vivo degradation of hydrogels

In vivo degradation of hydrogels was evaluated subcutaneously with male Sprague–Dawley rats (SD rats, 200–220 g; $n = 4$ rats/group) as previously reported [36]. As shown in Fig. 5a, first, the mediodorsal skin of SD rats was incised (1 cm in length), and a small lateral subcutaneous pocket was prepared. Then, GelMA, G-A-l, and G-A-L-i hydrogels ($n = 4$/group, 10 mm × 4 mm cylinders) were prepared and implanted into the subcutaneous pocket of SD rats under anesthesia conditions, and the gap was sutured quickly. Finally, the rats were sacrificed at 1, 2, 4, and 8 weeks post-surgery for hematoxylin-eosin (H&E) staining for histological analysis.

### 2.8. In vivo full-thickness skin defect healing experiments

First, a full-thickness skin defect model of the backs of SD rats was constructed. Briefly, after anesthesia, the mediodorsal skin was cleaned and disinfected with 2% iodophor, and a full-thickness skin wound model (a circle with a diameter of approximately 2 cm) was made in the depilated area of SD rats. Then, hydrogels were injected into the wounded area, and in situ gelling was formed through UV crosslinking and/or ionic crosslinking. Finally, the process of wound healing was traced by imagery and calculated using Image-J 1.45 software. At designated time intervals (4, 7, 14, and 21 days), the rats were sacrificed for H&E and Masson trichromatic staining for histological analysis. The group without any treatment was set as a control. As shown in Fig. S4, UV crosslinking was performed for GelMA and G-A-l hydrogels, G-A-L-i-1 was subjected to UV crosslinking and ion crosslinking superficially (a sponge filled with $CaCl_2$ solution covered the surface for 10 s), and UV crosslinking and ion crosslinking were performed for G-A-L-i-2 hydrogels ($CaCl_2$ solution was applied to the surface for 120 s). The process of UV crosslinking was carried out by applying UV at a wavelength of 365 nm (30 mW/cm$^2$) for 60 s.

### 2.9. Study approval

Collection of the synovial fluid samples from donors and all the animal experiments were approved by the Ethics Committee of Shenzhen University.

### 2.10. Statistical analysis

All the samples used in all the measurements were measured in quadruplicate, and the data are expressed as the means ± standard deviations (SDs). Statistical analysis was carried out via Tukey's post hoc test and one-way analysis of variance. Student's t-test was performed by SPSS software, and $^{*}p < 0.05$, $^{**}p < 0.01$ and $^{***}p < 0.001$ were considered to denote statistical significance.

## 3. Results and discussion

### 3.1. Fabrication and characterization of biomimetic hydrogels with a triple-network

To construct a biomimetic hydrogel with strong adjustable mechanical and tissue adhesion properties, here, a novel strategy of constructing a triple-network hydrogel with UV light-crosslinkable GelMA [42,43] and UV light-responsive Alg-NB [44] was designed. First, $^1$H NMR spectra were obtained to demonstrate the conjugation of MA to gelatin and NB to alginate. As Fig. 1c shows, for GelMA, 28.79% of the degree of methacrylation of gelatin was calculated (Fig. 1c), which was suitable for leaving some amino groups available to react with light-generated aldehyde groups [28,44]. For Alg-NB, the degree of NB substitution of Alg was approximately 13.25% (Fig. 1d), which was relatively low and was suitable for ionic crosslinking. In our previous works, we suggested that a low concentration of GelMA of 5 wt% was suitable for the application of soft tissues [28,40], therefore, the concentration of GelMA was set as 5 wt% throughout this work.

After GelMA and Alg-NB were successfully prepared, via UV-365 irradiance and the photopolymerization initiator LAP, the rheological characteristics of biomimetic hydrogels were measured. As shown in Fig. 2a, the chemically crosslinked GelMA/LAP hydrogel was rapidly formed (gel point = 2.24 ± 0.35 s; UV crosslinking time = 54.93 ± 5.24 s) with UV irradiation, and the final torsion modulus G' was approximately 22.4 ± 4.0 Pa, indicating that the first network structure could be formed between the GelMA polymers, which can contribute to the polycondensation of methacrylic anhydride [45,46]. In fact, the deficiencies of weak and brittle mechanical properties of GelMA precluded its application as a wound healing scaffold [42]. Moreover, in the addition of Alg to the GelMA/LAP hydrogel, the final torsion modulus G' improved to 153.2 ± 2.1 Pa (Fig. 2b). In the absence of LAP, GelMA/Alg-NB has a longer gelation time (gel point = 44.05 ± 0.83 s; UV

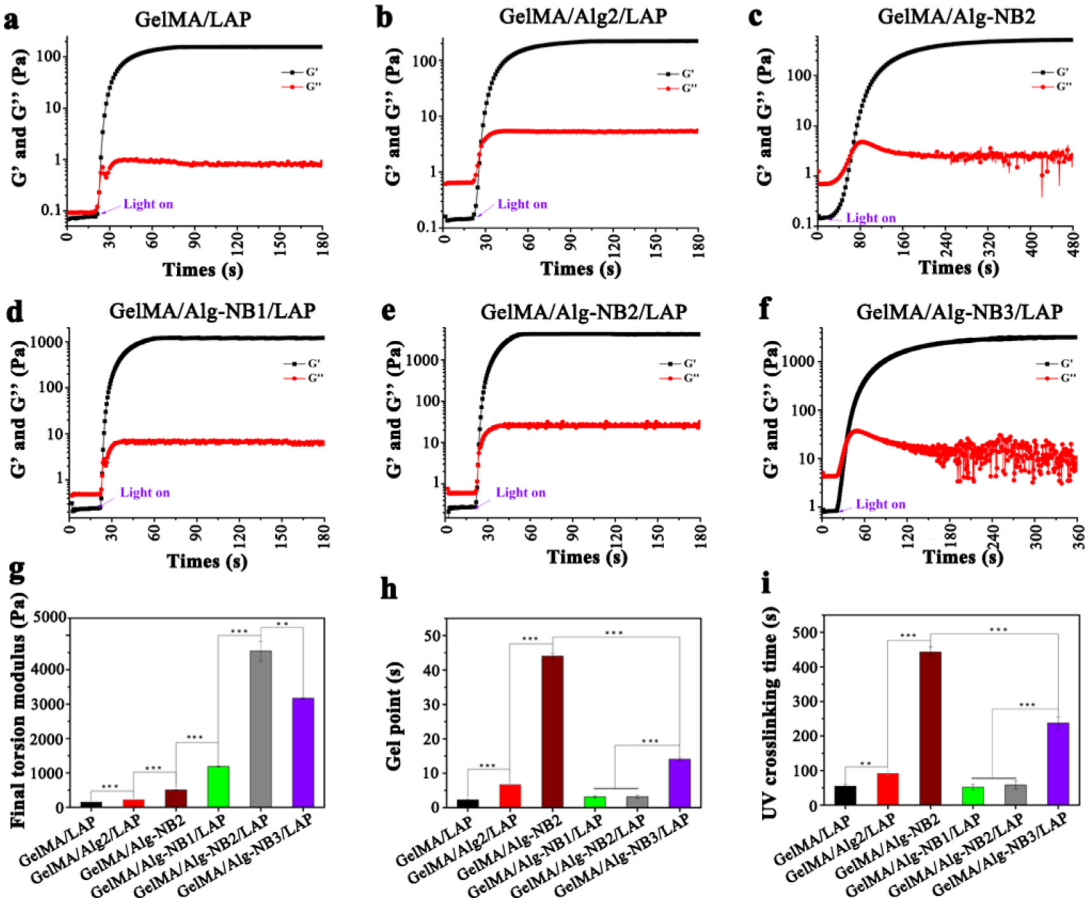


**Fig. 2.** Rheological properties test of different hydrogels, a dynamic time-sweep rheological analysis was used to monitor the gelling process. In situ photo-rheometer showing the formation kinetics for (a) GelMA/LAP, (b) GelMA/Alg2/LAP, (c) GelMA/Alg-NB2, (d) GelMA/Alg-NB1/LAP, (e) GelMA/Alg-NB2/LAP, (f) GelMA/Alg-NB3/LAP. Statistical results of the final torsion modulus G' (g), gel point (h), and UV crosslinking time (g) for different hydrogels. All the concentration of GelMA and LAP was set as 5 wt% and 0.1 wt%, respectively, and the ratio for Alg-NB:GelMA ratio were 1:10, 1:5 and 1:2.5 (corresponding groups were 1, 2 and 3), all the gelling measurements were conducted using OmniCure S2000 (365 nm, 30 mW/cm$^2$).

crosslinking time = 443.14 ± 15.05 s), but its mechanical properties are significantly improved (Fig. 2c), indicating that GelMA and Alg-NB can also form the second network connections, which can contribute to the dynamic covalent bond-Schiff bases between GelMA and Alg-NB. For GelMA/Alg-NB/LAP, the GelMA/Alg-NB2/LAP group maintained the characteristics of rapid gelation (gel point = 3.14 ± 0.46 s; UV crosslinking time = 51.86 ± 7.74 s), and its mechanical properties were greatly improved (Fig. 2e), which could be achieved by the dual-reaction of polycondensation of methacrylic anhydride and covalent bond-Schiff bases between GelMA and Alg-NB. With the increase in the concentration of Alg-NB in the GelMA/Alg-NB/LAP colloidal precursor, its final torsion modulus G' first increased and then decreased, the 1:10 ratio (GelMA/Alg-NB/LAP) resulted in hydrogels with the lowest G' (1189.7 ± 19.2 Pa), however, when the ratio of Alg-NB to GelMA higher than a threshold value, the superfluous Alg-NB may have a drawback for the mechanical properties of hydrogels, as Fig. 2d-g shown, the highest G' value was reached at the GelMA/Alg-NB2/LAP group (4542.3 ± 285.9 Pa), which was approximately 30-fold that of the GelMA/LAP group. Therefore, the concentrations for GelMA and Alg-NB in the next experiments were 5 wt% and 1 wt%, respectively. These results show that, compared with those of the GelMA/LAP hydrogel, the mechanical properties of the GelMA/Alg-NB/LAP hydrogel were greatly improved, and the latter could form a gel rapidly in a matter of seconds in the presence of the LAP initiator (Fig. 2h, i).

The compressive properties of hydrogels, referring to their elastic properties, are also one of their important mechanical properties. As shown in Fig. 3a, b, the elastic modulus of G-A-l was significantly higher than that of GelMA, peaking at 536.2 ± 6.0 kPa. This result shows good agreement with the rheological properties test results. Moreover, the elastic modulus of G-A-ʟ-i was significantly higher than that of GelMA and G-A-l, which can be attributed to ionic crosslinking of the Alg polymer chain, indicating that a triple-network was formed for the G-A-ʟ-i hydrogel. Taken together, all these results demonstrated that the biomimetic hydrogel with GelMA and Alg-NB can form a triple-network structure through UV crosslinking and ionic crosslinking, and the hydrogel of G-A-ʟ-i had superior mechanical properties.

Measuring the swelling properties of hydrogels is important for their biological applications, such as the sorption capacity of hydrogels, thus predicting the rate of degradation properties [36,47]. The swelling ratios of GelMA and G-A-ʟ-i were similar, and the swelling ratio of G-A-l was significantly higher than that of GelMA and G-A-ʟ-i (Fig. 3c; Fig. S2). From the statistical results of the swelling area change rate, it can be seen that the swelling area of G-A-ʟ-i has the smallest change rate, while that of G-A-l has the largest change. This result may be caused by the high crosslinking density of the G-A-ʟ-i hydrogel.

Considering the photogenerated aldehyde groups feature UV-sensitive NB micromolecules [48] and rich amino groups on the tissue surface [49], it can be expected that the G-A-ʟ-i hydrogel

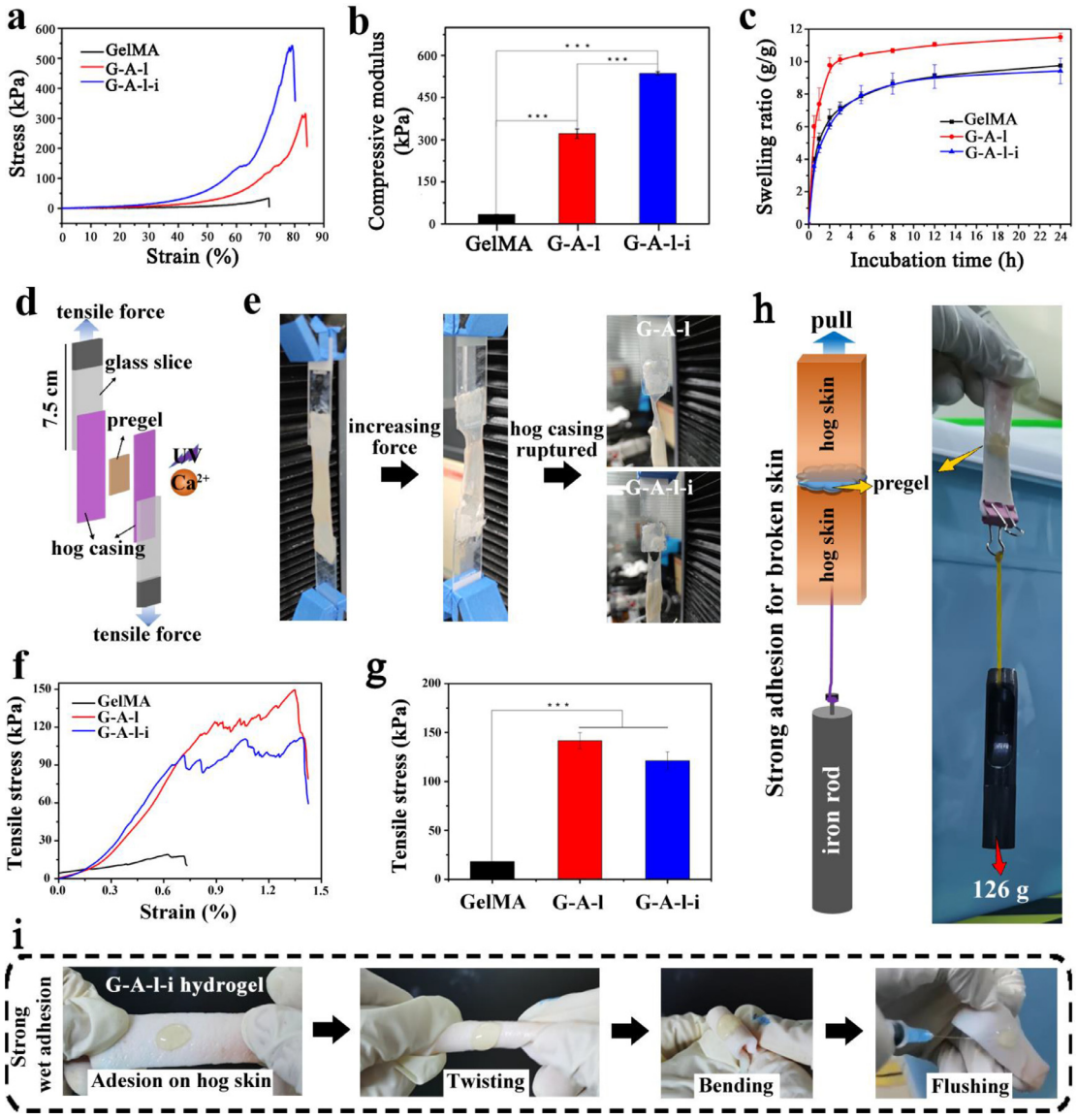


**Fig. 3.** Evaluation of the mechanical performance, tissue adhesive strength and swelling properties of the GelMA, G-A-l, and G-A-L-i hydrogels. (a) Stress–strain profile of hydrogels; (b) Compressive moduli of hydrogels; (c) The swelling ratio of different hydrogels, and the mass and area at 0 h was set as initial value; (d) Schematic diagram of the two lap-shear adhesion measurement to test the hydrogel–tissue binding strength; (e) The diagram of tissue adhesive strength test process; (f) Tensile stress–strain profile for evaluate the tissue adhesive of hydrogels; (g) The tissue adhesive strength of the hydrogels; (h) Schematic of the wound closure test for G-A-L-i hydrogel, and the images of the adhesion stretch resistance measurement process, the suspended iron rod is about 126 g; (i) No breakage or detachment between the G-A-L-i hydrogel and hog skin is seen in the photographs, stretch, twist, bend, and flush were carried to test the hydrogel–tissue binding strength. The concentration of GelMA and Alg-NB was set as 5 wt% and 1 wt%, respectively, the intensity of UV365 was 30 mW/cm$^2$, and irradiated for 60 s.

had an excellent tissue adhesion ability. As shown in Fig. 3d, the tissue adhesion of hydrogel was explored, transparent pig casings were used to simulate tissue, and the adhesive tensile force between molecular glue and tissue material was tested by a universal testing machine. Compared with that of the GelMA hydrogel, the tissue adhesive strength of the G-A-l and G-A-L-i hydrogels significantly improved (Fig. 3e-g). In fact, when the tensile force of the universal testing machine was constantly improved, even if the pig casings were damaged, the bonding of G-A-l and G-A-L-i hydrogels with tissue still very good (Fig. 3d). Moreover, the G-A-L-i hydrogel shows an decent wound closure effect (Fig. 3h), and no breakage or detachment between the hydrogel and tissue was seen (Fig. 3i). These results proved that the designed triple-network hydrogel shows good tissue adhesion performance. In our previous work, we proved that the high tissue adhesion of matrix gels containing NB was derived from photogenerated aldehyde groups bonding with the amino groups on the tissue surface [28,50,51]. Taken together, the above results demonstrated that the G-A-L-i hydrogel formed a triple- network and that the high crosslinking density of the G-A-L-i hydrogel contributed to its strong mechanical properties, wet tissue adhesion, and low swelling ratio.

### *3.2. In vitro evaluation of biocompatibility for biomimetic hydrogels with a triple-network*

Although GelMA-based and alginate-based polymers have been widely used for skin repair, their biocompatibility has been well proven, as they closely resemble some essential properties of native ECM [46,52]. Nevertheless, as an in situ forming hydrogel for GelMA/Alg-NB/LAP, it is still necessary to demonstrate the biocompatibility of this modified and composite hydrogel. To evaluate the biocompatibility of hydrogels and the ability of cells to grow in-

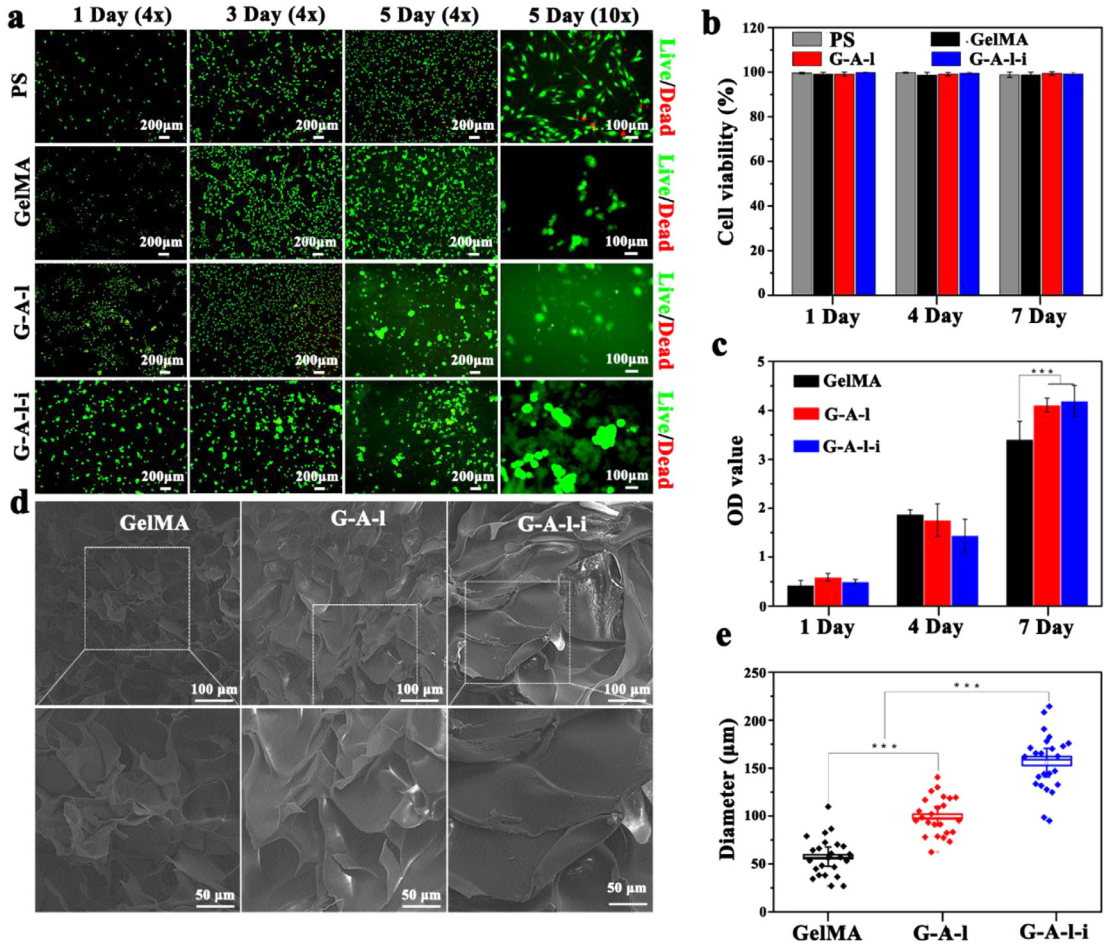


**Fig. 4.** Cytotoxicity of the hydrogel materials and the internal morphology of GelMA, G-A-l and G-A-L-i hydrogels. (a) Live/Dead staining of HSFs after cultured on the surface of different hydrogels for 1, 3 and 5 days, calcein AM for live cells (green) and ethidium homodimer-1 for dead cells (red), PS substrate was carried out as control group; (b) Cell viability quantification of HSFs cultured on the surface of different hydrogels; (c) Cell proliferation measured with CCK-8 assay after HSFs cultured on the surface of hydrogels for 1, 4 and 7 days; (d) SEM images shows the internal porous structure morphology for hydrogels; (e) Quantitative analysis of pore size in hydrogels using software of Image-J 1.45 system.

ward on the surface of the hydrogels, HSFs were inoculated on the surface of hydrogels to investigate the cell viability and proliferation behavior of HSFs cells, and live/dead staining and CCK-8 assay were carried out.

Fig. 4a shows the viability of HSFs on GelMA, G-A-l, and G-A-L-i hydrogels. Cells seeded on blank PS substrates were used to simulate a two-dimensional (2D) culture environment. After the cells were cultured for 1, 3 and 5 days, all the samples presented superficial cell viability (Fig. 4b). The images of live/dead staining show that HSFs proliferate rapidly over time, and the results of the CCK-8 method for HSFs cultured on the surface of hydrogels confirmed this conclusion (Fig. 4c). Notably, as the photograph in Fig. 4a shows, the cells adhered and proliferated on the 2D surface of the PS substrate uniformly. For the GelMA and G-A-l groups, cells continued to grow in two dimensions within 3 days but exhibited cell clusters on the 5th day, which indicated that cells grew in three dimensions, and GelMA and G-A-l hydrogels functioned as a 3D cell culture scaffold. Moreover, on the surface of the G-A-L-i hydrogel, cells grew into clusters on the 1st day, the size of the clusters increased constantly, and the phenomenon of growing into clusters of cells was much more obvious than that on GelMA and G-A-l hydrogels. Many reported works have proven that 3D cell clusters are more conducive to cell expansion and transplantation due to their high surface growth space, which equates to an excellent advantage for organizational reconstruction [53,54]. These results demonstrated that the biomimetic hydrogel with a triple-network had excellent biocompatibility and could function as a 3D scaffold for cell proliferation and tissue regeneration.

As the results of live/dead staining show, there were distinct differences in cell morphology between the GelMA, G-A-l, and G-A-L-i hydrogels, which may be attributed to the porous structure of the hydrogels. As such, the microscopic structures of the hydrogels were measured using scanning electron microscopy (SEM). As the SEM results show, the GelMA, G-A-l, and G-A-L-i hydrogels all have a significantly porous structure (Fig. 4d); moreover, the pore sizes of the GelMA, G-A-l, and G-A-L-i hydrogels significantly increased sequentially; the pore sizes were 56.7 ± 18.2 $\mu$m, 96.0 ± 19.7 $\mu$m, and 160.1 ± 28.9 $\mu$m, respectively (Fig. 4e). In fact, the diameter of most cultured animal-derived cells was approximately 10–100 $\mu$m [55–57], which indicated that HSFs seeded on the surface of G-A-L-i hydrogels can be readily captured by the pore structure and grow into cell clusters. Moreover, considering the fact that GelMA, G-A-l, and G-A-L-i hydrogels all cannot be degraded in vitro within 5 days (Fig. S3), G-A-l hydrogel and G-A-L-i hydrogel have the similar biochemical composition, Alg-NB was a modified products by alginate (alginate precludes cell adhesion), and the most different for G-A-l hydrogel and G-A-L-i hydrogel was the macroporous microstructure, therefore, the most possible reason for phenomenon of cells grew into clusters on the surface of G-A-L-i hydrogel can be contributed to its macroporous architecture. These results demon-

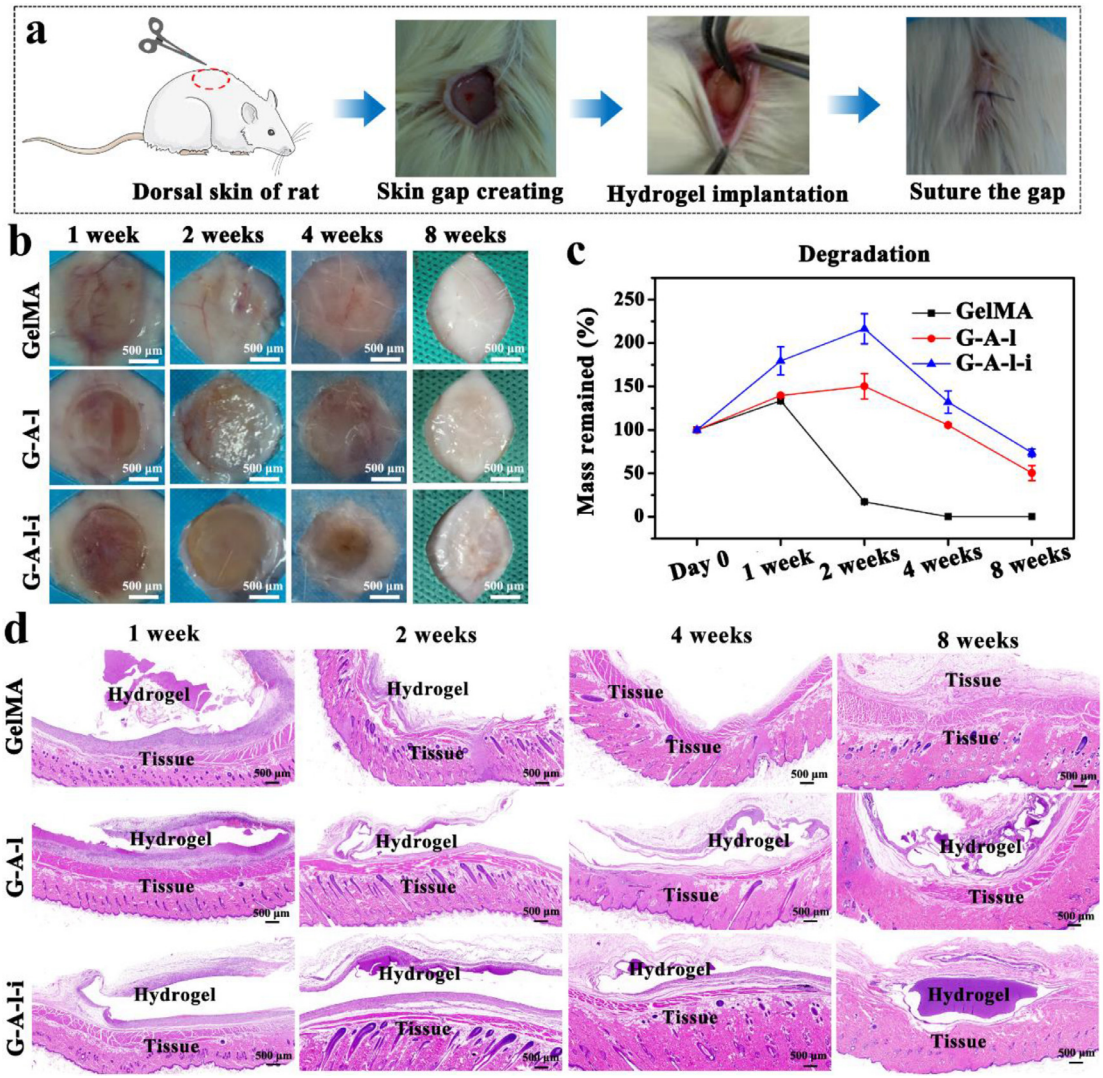


**Fig. 5.** In vivo biodegradability analysis of GelMA, G-A-l and G-A-L-i hydrogels. (a) Diagram of hydrogels transplanted process; (b) Hydrogels transplanted into the subcutaneous space of SD rats were collected after 1, 2, 4 and 8 weeks; (c) Mass retention of different hydrogels after various weeks in vivo, the mass of hydrogels were estimated by volume; (d) Hematoxylin/eosin staining of subcutaneously implanted GelMA, G-A-l and G-A-L-i hydrogels at 1, 2, 4 and 8 weeks. The hydrogels were filled in the blank area of the cavity, and hydrogels in some groups may split away off during the process of section staining.

strated that the G-A-L-i hydrogel had a 3D microstructure with a macroporous architecture, which could facilitate cell migration and proliferation to cell clusters in the 3D direction and shows promise for tissue regeneration applications.

### *3.3. In vivo evaluation of biodegradability for biomimetic hydrogels with a triple-network*

GelMA, G-A-l, and G-A-L-i hydrogels were dorsally subcutaneously implanted in an SD rat model to evaluate the biodegradability and biocompatibility of the hydrogel in vivo (Fig. 5a), and the incubated hydrogels were surgically harvested at the 1st, 2nd, 4th, and 8th weeks. A tendency of swelling first and subsequent degradation was observed for all the hydrogels (Fig. 5b, c), which corresponded to the results of the in vitro evaluation of the biodegradability of the hydrogels (Fig. S3), suggesting the high water content and biodegradability of the hydrogels [58]. Matrix components of GelMA hydrogel with a low concentration (5 wt%) degraded rapidly and fused with tissue within one week and almost completely degraded at 2nd week. Nevertheless, the swelling process for G-A-l and G-A-L-i hydrogels extended to the 2nd week and slowly degraded afterward. Apparent residues could be perceived within the testing, which demonstrated the excellent water content and slow degradation properties for G-A-l and G-A-L-i hydrogels, and the G-A-L-i hydrogel had the slowest degradation ratio, which might be explained by their multiple network crosslinking and the modified alginate is inherently slow-degradable in mammals [52]. It was reported that hydrogels with a slow degradation profile are more conducive to the inward growth of cells and promote tissue growth to replace implants [36,59], thus, the G-A-L-i hydrogel might be more suitable for full-thickness skin defect repair. In addition, after hydrogel implantation, there was a slight inflammatory reaction in the early stage (before the 1st week), and the inflammatory reaction gradually disappeared in the later stage (after the 2nd week), indicating that all the hydrogels have good biocompatibility.

Moreover, H&E staining of subcutaneous GelMA hydrogels showed noninflammatory tissue progressive ingrowth from the recipient into the samples at one week and complete absorption at the 2nd week (Fig. 5d), indicating biocompatibility and quick degradation of the GelMA hydrogel in vivo. The H&E results also demonstrated that minimal inflammation occurred in vivo as a result of the subcutaneous G-A-l and G-A-L-i implants, and the G-A-l and G-A-L-i hydrogels slowly integrated with noninflammatory tis-

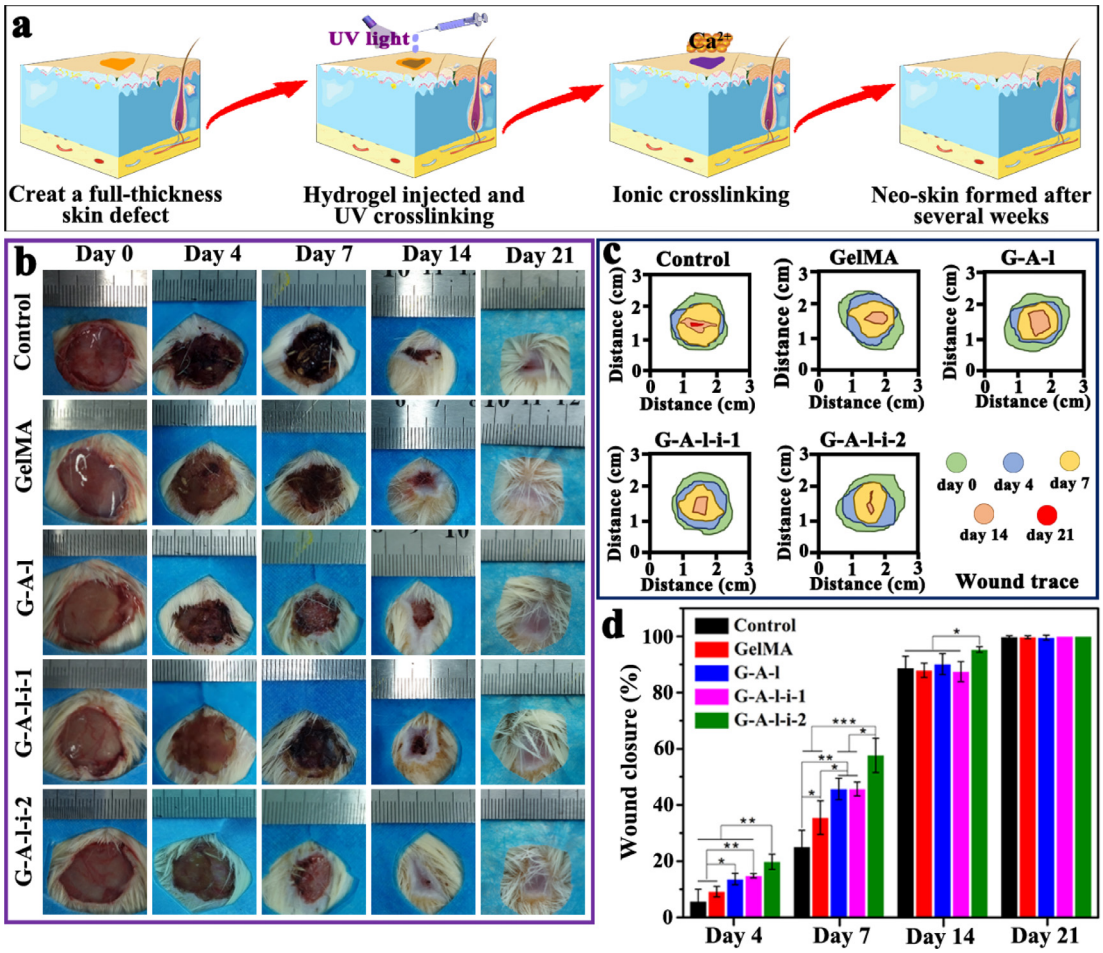


**Fig. 6.** Biomimetic hydrogel for full-thickness skin defect repair in rat model. (a) Schematic representation of the surgical process. Full-thickness defects were created on the dorsal surface of SD rats and hydrogels were injected into the wounded area and in situ gelling was formed, UV-crosslinking for GelMA and G-A-l hydrogels, G-A-L-i-1was treated with UV light and ion crosslinking on its superficial, UV and ion crosslinking for G-A-L-i-2 hydrogels; (b) Photographs of wounds at 4, 7, 14 and 21 days for treated with GelMA, G-A-l, G-A-L-i-1 and G-A-L-i-2, repectively, the untreated group was functioned as the control group; (c) Traces of wound-bed closure during 21 days for each treatment; (d) Percentage of wound closure for each treatment on day 4, 7, 14 and 21 post-operation.

sue within 8 weeks (Fig. 5d), suggesting biocompatibility and slow degradation of G-A-l and G-A-L-i hydrogels in vivo. All these results demonstrated the biocompatibility and slow degradation characteristics of the designed G-A-L-i hydrogel with a triple-network structure. Indeed, the noninflammatory response and slow degradation properties are crucial for stopping hemorrhage, adequately sealing internal tissue defects, and promoting moderate tissue ingrowth [59,60], indicating good application potential for tissue repair.

### *3.4. In vivo full-thickness skin repair using biomimetic hydrogel with a triple-network*

A mouse full-thickness dorsal skin defect model was employed to evaluate the wound healing ability of the G-A-L-i hydrogel (Fig. 6). A schematic diagram of the wound repair procedure is shown in Fig. 6a. A full-thickness skin defect with a diameter of approximately 2 cm on the dorsal surface was created, and a triple-network G-A-L-i hydrogel was injected into the cutaneous defect and formed in situ with UV crosslinking and ionic crosslinking. Neo-skin formed after several weeks. The group without treatment was set as a blank control, and GelMA, G-A-l, and G-A-L-i-1 (bottom: double network, surface: triple network) hydrogels were used to compare the repair effects with different crosslinking pathways (Fig. S4). To realistically simulate the full-thickness skin defect repair process, the hair of the SD rats were not shaven [61,62].

The wound healing process was monitored photographically at 4, 7, 14 and 21 days post-wounding (Fig. 6b). The wounds quickly closed without the need for suture in all the groups with hydrogels compared with the untreated control group, preventing further bleeding and preventing potential bacterial infections (Fig. S5). In fact, the treatments of hydrogels all showed significantly increased wound healing; among them, the effect accelerated wound repair for G-A-L-i-2 hydrogel with triple-network was the best, and the wound closure ratio reached 57.7 ± 6.1 on the 7th day and 95.3 ± 1.0 on the 14th day. The wounds closed completely by the 21st day for all the groups (Fig. 6c, d). Normally, connective tissue hyperplasia builds up on the wounded area after trauma [63]. As shown in Fig. 6b, connective tissue could be distinctly observed for the control group, and slightly occurred for GelMA, G-A-l, and G-A-L-i-1 groups; however, the surface remained flat and smooth within the wound closure process for G-A-L-i-2 hydrogel with triple-network, as connective tissue hyperplasia could eventual maturation into scar tissue [64], which indicated GelMA/Alg-NB/LAP hydrogel with triple-network could be used to reduce the likelihood of scarring and even functioned as a tissue-engineered skin for wound repair. All these results indicate the high efficiency and quality full-thickness skin defect repair for the GelMA/Alg-NB/LAP hydrogel with a triple-network.

Subsequently, microscopy examination with hematoxylin–eosin staining (H&E staining) was employed to evaluate the neotissue

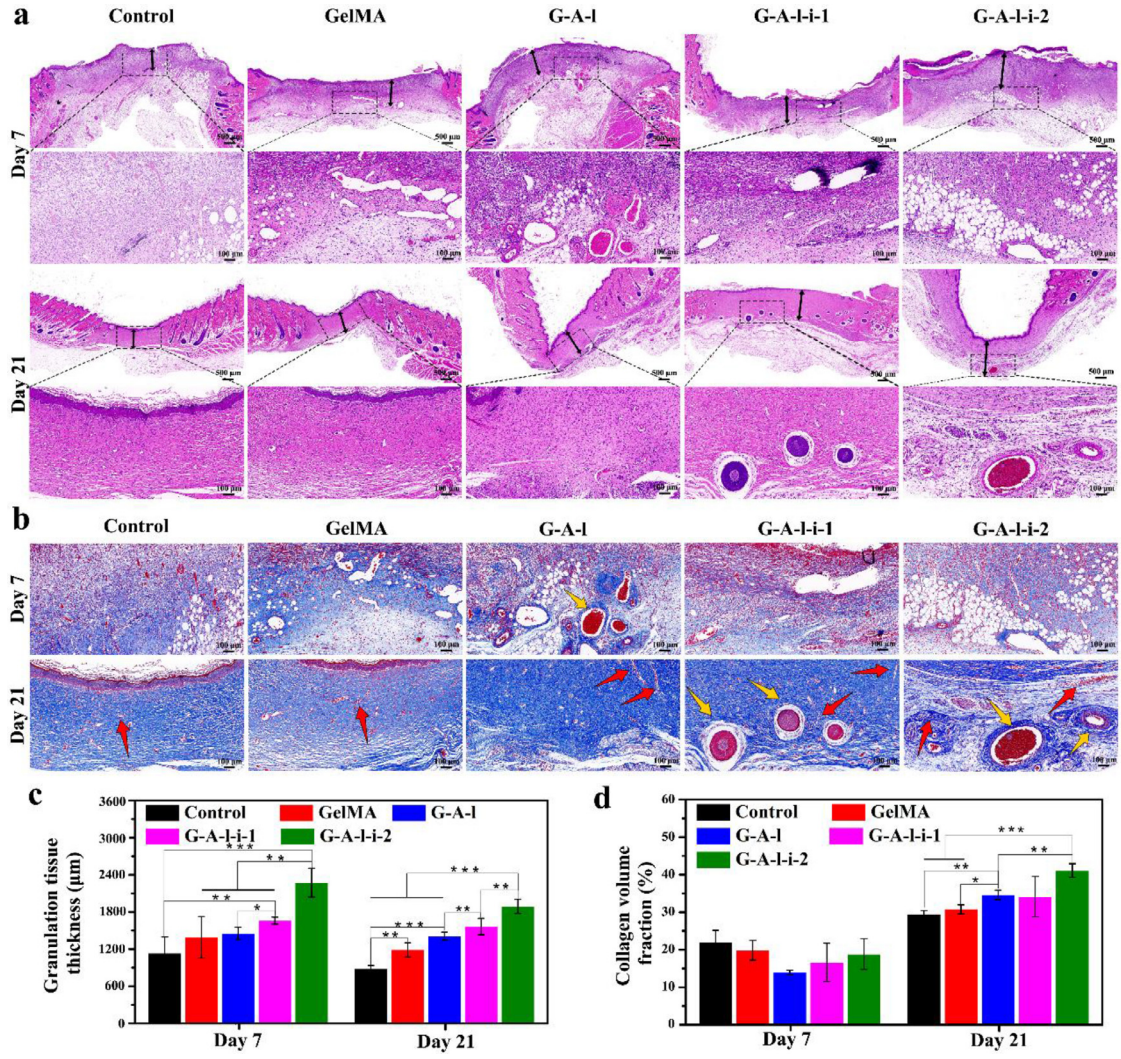


**Fig. 7.** Analysis of healed wounds. (a) H&E staining evaluation of wound regeneration for GelMA, G-A-l, G-A-L-i-1 and G-A-L-i-2 hydrogels on 7th and 21st day; (b) Masson staining evaluation of wound regeneration for GelMA, G-A-l, G-A-L-i-1 and G-A-L-i-2 hydrogels on 7th and 21st day (blood vessels: red arrows, hair follicles: yellow arrows); (c) Quantification of granulation tissue thickness for different treatments on 7th and 21st measured in H&E's trichrome stained tissue sections; (d) Quantification of collagen volume fraction for different treatments on 7th and 21st measured in Masson's trichrome stained tissue sections, light blue color corresponded to the collagen deposition.

formation progress at different time points. H&E staining showed that the granulation tissue consisted of some growth factors and abundant fibroblasts [63] filling the wound on the 4th day and gradually forming the basic structure of the epithelium and dermis on the 21st day (Fig. 7a, Fig. S6a). To quantitatively evaluate the wound healing process, the granulation tissue thickness was measured with Image-J software [65]. As shown in Fig. 7c and Fig. S6c, the granulation tissue thickness of all the hydrogel-coated groups was significantly thicker than that of the untreated control group in different phases, and the group of triple-network G-A-L-i-2 hydrogels was the optimal one. These results further demonstrated that the GelMA/Alg-NB/LAP hydrogel with a triple-network could accelerate full-thickness skin defect repairs efficiently.

Furthermore, microscopy examination of Masson's trichrome staining was carried out to evaluate the quality of the healing process Fig. 7.b and Fig. S6b show that capillary vessels were visible in all the groups and were particularly obvious for the G-A-L-i-1 and G-A-L-i-2 hydrogel groups, as angiogenesis or new blood vessel formation is an important marker of wound healing [66,67], and robust capillary growth indicated the normal wound healing of the GelMA/Alg-NB/LAP hydrogel. Moreover, after 14 days, the rats in the G-A-L-i-1 and G-A-L-i-2 hydrogel groups exhibited more hair follicles than did those in the other groups did, and hair follicles were also observed in the granulation tissue. In addition, it was found that the G-A-L-i-2 hydrogel group presented accelerated collagen deposition in the wound healing model compared to the four other treatment groups, and the collagen volume fraction was approximately 41.1 ± 1.8% in the G-A-L-i-2 hydrogel group (Fig. 7d and Fig. S6d).

Conventionally, cytokines are closely related to the cell metabolism and proliferation behaviors for wound healing [68], and the influence of the G-A-L-i hydrogel on angiogenesis in skin wounds was also analyzed. Immunohistochemical staining for CD31 to evaluate the neovascularization in the early vascular remodeling stage of wound healing [69], and stained for $\alpha$-SMA to observe the vascular networks with smooth muscle cells (SMCs) [40]. As shown in Fig. 8a-c, CD31 staining and $\alpha$-SMA staining were all significantly increased in the groups with hydrogels when compared to the control group, and the G-A-L-i-2 hydrogel group obtained the highest expression, that further demonstrated the ability to promote capillary vessels and angiogenesis formation for the G-A-L-i-2 hydrogel with a triple-network. In general, these results demonstrated that mature granulation and dermis formed with skin appendages (including hair follicles and blood vessels)

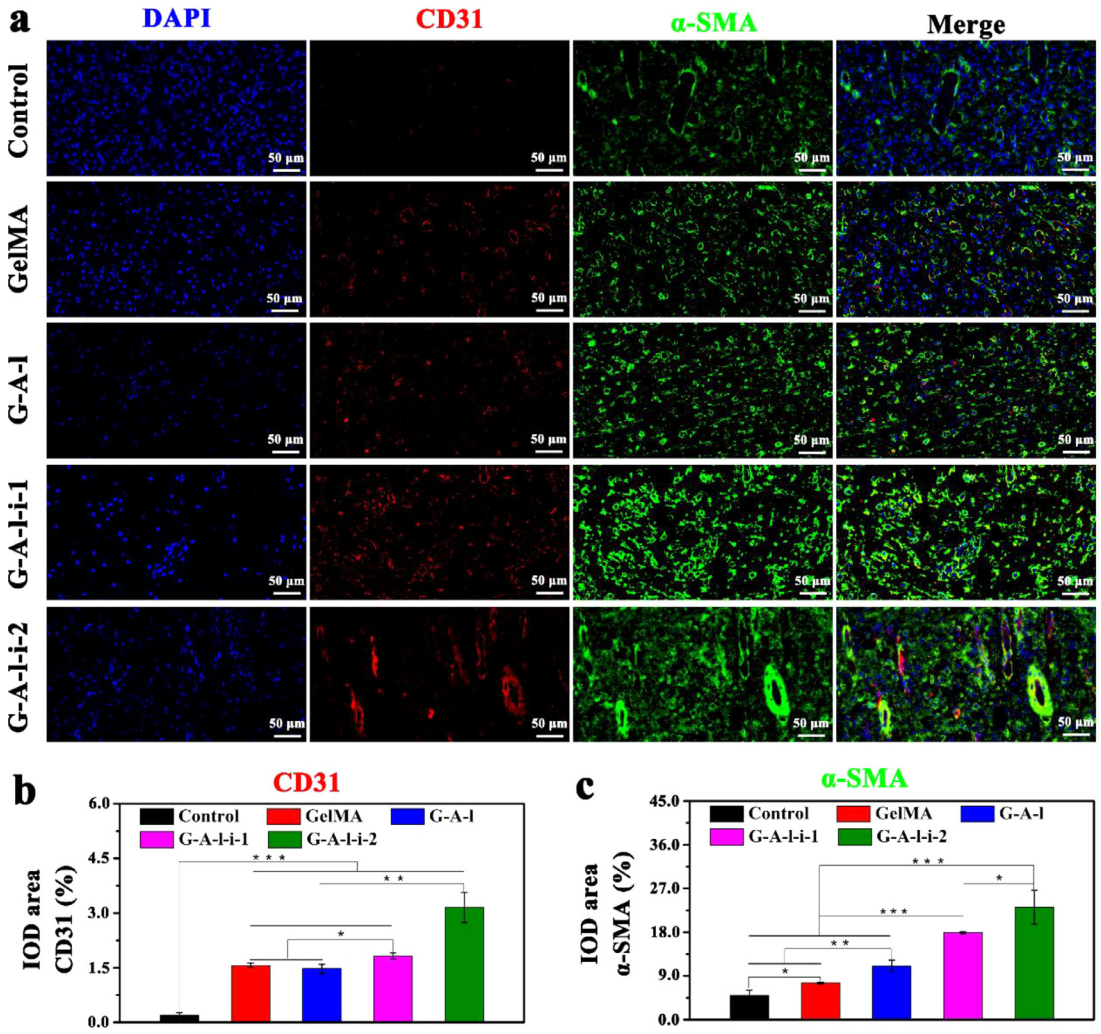


**Fig. 8.** Immunohistochemical staining of nuclei and angio-biomarkers for skin wounds on 7th day after treatment. (a) Immunostained for CD 31 (red) and $\alpha$-SMA (green); (b) Quantification of (c) CD 31 and (d) $\alpha$-SMA staining of the wound areas by Image J software (IOD is the mean integrated optical density).

in the GelMA/Alg-NB/LAP hydrogel group, which indicated a high efficiency and quality full-thickness skin defect repairing ability.

Therefore, triple-network GelMA/Alg-NB/LAP hydrogels have strong mechanical properties, exert wet tissue adhesion, undergo slow biodegradation, and have macroporous microstructures and could function as tissue-engineered skin with biocompatible, biodegradable, noncytotoxic, and nonimmunogenic properties. These hydrogels could be utilized to accelerate the full-thickness skin defect repair process by reducing the infection through rapid sutureless wound closure, promoting tissue ingrowth. Such characteristics make the triple-network GelMA/Alg-NB/LAP hydrogel a suitable UV-ionic-crosslinking injectable hydrogel for potential biomaterial scaffolds to promote local neoskin formation through simple injection and in situ formation. Moreover, such mechanical properties and biological activity make this biomimetic hydrogel show potential application in hemostasis, cartilage defects, and even organ manufacturing.

## 4. Conclusion

In summary, a GelMA/Alg-NB/LAP hydrogel with a triple-network structure was fabricated through UV crosslinking and ionic crosslinking and showed superior mechanical properties, tissue adhesion abilities, macroporous microstructures, and biological activities. Furthermore, in vitro cell activity assessments proved that the triple-network biomimetic hydrogel had excellent biocompatibility and could function as a 3D scaffold for cell proliferation. Additional in vivo measurements demonstrated its biocompatibility and slow biodegradation and that this hydrogel was very suitable for utilization as a scaffold for full-thickness skin defect repair. Such biomimetic hydrogels provide new ideas and strategies for the clinical application of quick sutureless wound closure and high-quality repair. In the future, we anticipate that more potential applications, such as hemostasis and cartilage defect repair, will be feasible based on this biomimetic hydrogel and its derived products.

## Declaration of Competing Interest

The authors declare no competing financial interest.

## CRediT authorship contribution statement

**Xiaojun Long**: Conceptualization, Methodology, Investigation, Resources, Data curation, Formal analysis, Writing – original draft, Writing – review & editing. **Xiao Xu**: Conceptualization, Methodology, Investigation, Formal analysis. **Deshun Sun**: Conceptualization, Methodology, Writing – original draft, Funding acquisition. **Yi Hong**: Conceptualization, Methodology, Investigation. **Caining**

**Wen**: Methodology, Investigation. **Yixin Xie**: Methodology, Investigation. **Bing Yan**: Conceptualization, Resources. **Huawei Zhang**: Methodology, Resources. **Qi Ge**: Methodology, Resources. **Wencui Li**: Conceptualization, Methodology, Writing – original draft, Writing – review & editing, Funding acquisition, Project administration. **Li Duan**: Conceptualization, Methodology, Writing – original draft, Writing – review & editing, Funding acquisition, Project administration. **Hongwei Ouyang**: Conceptualization, Supervision, Funding acquisition, Project administration, Writing – review & editing. **Daping Wang**: Conceptualization, Supervision, Funding acquisition, Project administration, Writing – review & editing.

## Acknowledgements

This work is supported by the Supported by Shenzhen High-level Hospital Construction Fund (SZGSP007), Shenzhen Institutes of Advanced Technology Innovation Program for Excellent Young Researchers (RCBS20200714114856171), National Natural Science of China under Grant (No.62103287), National Natural Science Foundation of China (81972085, 82172465). The authors thank Mr. Chao Fang for the SEM imaging, Miss Xiangnan He for the help of rheological analysis, professor Qianjun He for the help of compressive moduli test.

## Reference

[1] M. Puthia, M. Butrym, J. Petrlova, A.C. Strömdahl, M.Å. Andersson, S. Kjellström, A. Schmidtchen, A dual-action peptide-containing hydrogel targets wound infection and inflammation, Sci. Transl. Med. 12 (2020) 1–15.
[2] L. Martinengo, M. Olsson, R. Bajpai, M. Soljak, Z. Upton, A. Schmidtchen, J. Car, K. Jarbrink, Prevalence of chronic wounds in the general population: systematic review and meta-analysis of observational studies, Ann. Epidemiol. 29 (2019) 8–15.
[3] M. Farokhi, F. Mottaghitalab, Y. Fatahi, A. Khademhosseini, D.L. Kaplan, Overview of silk fibroin use in wound dressings, Trends Biotechnol 36 (2018) 907–922.
[4] N. Annabi, D. Rana, E. Shirzaei Sani, R. Portillo-Lara, J.L. Gifford, M.M. Fares, S.M. Mithieux, A.S. Weiss, Engineering a sprayable and elastic hydrogel adhesive with antimicrobial properties for wound healing, Biomaterials 139 (2017) 229–243.
[5] P. Martin, Wound healing—Aiming for perfect skin regeneration, Science 276 (1997) 75–81.
[6] X. Zhao, Y. Liang, Y. Huang, J. He, Y. Han, B. Guo, Physical double-network hydrogel adhesives with rapid shape adaptability, fast self-healing, antioxidant and NIR/pH stimulus-responsiveness for multidrug-resistant bacterial infection and removable wound dressing, Adv. Funct. Mater. 30 (2020) 1910748.
[7] S. MacNeil, Progress and opportunities for tissue-engineered skin, Nature 445 (2007) 874–880.
[8] V.L. Negenborn, D.A. Young-Afat, R.E.G. Dikmans, J.M. Smit, H.A.H. Winters, J.P.W. Don Griot, J.W.R. Twisk, P.Q. Ruhé, M.A.M. Mureau, O. Lapid, E. Moerman, A.A.W.M. van Turnhout, M.J.P.F. Ritt, M.B. Bouman, M.G. Mullender, Quality of life and patient satisfaction after one-stage implant-based breast reconstruction with an acellular dermal matrix versus two-stage breast reconstruction (BRIOS): primary outcome of a randomised, controlled trial, Lancet Oncol. 19 (2018) 1205–1214.
[9] T. Cui, J. Yu, Q. Li, C.F. Wang, S. Chen, W. Li, G. Wang, Large-scale fabrication of robust artificial skins from a biodegradable sealant-loaded nanofiber scaffold to skin tissue via microfluidic blow-spinning, Adv. Mater. 32 (2020) e2000982.
[10] K.M. Kulig, X. Luo, E.B. Finkelstein, X.H. Liu, S.M. Goldman, C.A. Sundback, J.P. Vacanti, C.M. Neville, Biologic properties of surgical scaffold materials derived from dermal ECM, Biomaterials 34 (2013) 5776–5784.
[11] S.Y. Wang, H. Kim, G. Kwak, H.Y. Yoon, S.D. Jo, J.E. Lee, D. Cho, I.C. Kwon, S.H. Kim, Development of biocompatible HA hydrogels embedded with a new synthetic peptide promoting cellular migration for advanced wound care management, Adv. Sci. 5 (2018) 1800852.
[12] C. Ghobril, M.W. Grinstaff, The chemistry and engineering of polymeric hydrogel adhesives for wound closure: a tutorial, Chem. Soc. Rev. 44 (2015) 1820–1835.
[13] Y. Liang, J. He, B. Guo, Functional hydrogels as wound dressing to enhance wound healing, ACS Nano 15 (2021) 12687–12722.
[14] H. Li, A.M. Koenig, P. Sloan, N.D. Leipzig, In vivo assessment of guided neural stem cell differentiation in growth factor immobilized chitosan-based hydrogel scaffolds, Biomaterials 35 (2014) 9049–9057.
[15] K.M. Park, J.A. Yang, H. Jung, J. Yeom, J.S. Park, K.H. Park, A.S. Hoffman, S.K. Hahn, K. Kim, In situ supramolecular assembly and modular modification of hyaluronic acid hydrogels for 3D cellular engineering, ACS Nano. 6 (2012) 2960–2968.
[16] T. Hao, J. Li, F. Yao, D. Dong, Y. Wang, B. Yang, C. Wang, Injectable fullerenol/alginate hydrogel for suppression of oxidative stress damage in brown adipose-derived stem cells and cardiac repair, ACS Nano. 11 (2017) 5474–5488.
[17] M. Kim, J.Y. Lee, C.N. Jones, A. Revzin, G. Tae, Heparin-based hydrogel as a matrix for encapsulation and cultivation of primary hepatocytes, Biomaterials 31 (2010) 3596–3603.
[18] Y. Liang, Z. Li, Y. Huang, R. Yu, B. Guo, Dual-dynamic-bond cross-linked antibacterial adhesive hydrogel sealants with on-demand removability for post–wound-closure and infected wound healing, ACS Nano. 15 (2021) 7078–7093.
[19] M.C. Giano, Z. Ibrahim, S.H. Medina, K.A. Sarhane, J.M. Christensen, Y. Yamada, G. Brandacher, J.P. Schneider, Injectable bioadhesive hydrogels with innate antibacterial properties, Nat. Commun. 5 (2014) 4095.
[20] H. Yuk, C.E. Varela, C.S. Nabzdyk, X. Mao, R.F. Padera, E.T. Roche, X. Zhao, Dry double-sided tape for adhesion of wet tissues and devices, Nature 575 (2019) 169–174.
[21] X. Peng, X. Xu, Y. Deng, X. Xie, L. Xu, X. Xu, W. Yuan, B. Yang, X. Yang, X. Xia, L. Duan, L. Bian, Ultrafast self-gelling and wet adhesive powder for acute hemostasis and wound healing, Adv. Funct. Mater. 31 (2021) 2102583.
[22] J. Shin, J.S. Lee, C. Lee, H.J. Park, K. Yang, Y. Jin, J.H. Ryu, K.S. Hong, S.H. Moon, H.M. Chung, H.S. Yang, S.H. Um, J.W. Oh, D.I. Kim, H. Lee, S.W. Cho, Tissue adhesive catechol-modified hyaluronic acid hydrogel for effective, minimally invasive cell therapy, Adv. Funct. Mater. 25 (2015) 3814–3824.
[23] Y. Yuan, S. Shen, D. Fan, A physicochemical double cross-linked multifunctional hydrogel for dynamic burn wound healing: shape adaptability, injectable self-healing property and enhanced adhesion, Biomaterials 276 (2021) 120838.
[24] E.S. Place, N.D. Evans, M.M. Stevens, Complexity in biomaterials for tissue engineering, Nat. Mater. 8 (2009) 457–470.
[25] J.S. Gonzalez, L.N. Luduena, A. Ponce, V.A. Alvarez, Poly(vinyl alcohol)/cellulose nanowhiskers nanocomposite hydrogels for potential wound dressings, Mat. Sci. Eng. C-Mater. Biol. Appl. 34 (2014) 54–61.
[26] J. Zhu, Bioactive modification of poly(ethylene glycol) hydrogels for tissue engineering, Biomaterials 31 (2010) 4639–4656.
[27] Y. Liang, X. Zhao, T. Hu, B. Chen, Z. Yin, P.X. Ma, B. Guo, Adhesive hemostatic conducting injectable composite hydrogels with sustained drug release and photothermal antibacterial activity to promote full-thickness skin regeneration during wound healing, Small 15 (2019) e1900046.
[28] Y. Hong, F. Zhou, Y. Hua, X. Zhang, C. Ni, D. Pan, Y. Zhang, D. Jiang, L. Yang, Q. Lin, Y. Zou, D. Yu, D.E. Arnot, X. Zou, L. Zhu, S. Zhang, H. Ouyang, A strongly adhesive hemostatic hydrogel for the repair of arterial and heart bleeds, Nat. Commun. 10 (2019) 2060.
[29] H. Qi, Y. Du, L. Wang, H. Kaji, H. Bae, A. Khademhosseini, Patterned differentiation of individual embryoid bodies in spatially organized 3D hybrid microgels, Adv. Mater. 22 (2010) 5276–5281.
[30] S.R. Shin, B. Aghaei-Ghareh-Bolagh, T.T. Dang, S.N. Topkaya, X. Gao, S.Y. Yang, S.M. Jung, J.H. Oh, M.R. Dokmeci, X.S. Tang, A. Khademhosseini, Cell-laden microengineered and mechanically tunable hybrid hydrogels of gelatin and graphene oxide, Adv. Mater. 25 (2013) 6385–6391.
[31] M. Tavafoghi, A. Sheikhi, R. Tutar, J. Jahangiry, A. Baidya, R. Haghniaz, A. Khademhosseini, Engineering tough, injectable, naturally derived, bioadhesive composite hydrogels, Adv. Healthc. Mater. 9 (2020) e1901722.
[32] D.R. Griffin, W.M. Weaver, P.O. Scumpia, D.D. Carlo, T. Segura, Accelerated wound healing by injectable microporous gel scaffolds assembled from annealed building blocks, Nat. Mater. 14 (2015) 737–744.
[33] L.H. Han, X. Tong, F. Yang, Photo-crosslinkable PEG-based microribbons for forming 3D macroporous scaffolds with decoupled niche properties, Adv. Mater. 26 (2014) 1757–1762.
[34] T.M.A. Henderson, K. Ladewig, D.N. Haylock, K.M. McLean, A.J. O'Connor, Cryogels for biomedical applications, J. Mater. Chem. B 1 (2013) 2682–2695.
[35] C. Fan, Y. Ling, W. Deng, J. Xue, P. Sun, D.A. Wang, A novel cell encapsulatable cryogel (CECG) with macro-porous structures and high permeability: a three-dimensional cell culture scaffold for enhanced cell adhesion and proliferation, Biomed. Mater. 14 (2019) 055006.
[36] F. Zhou, Y. Hong, X. Zhang, L. Yang, J. Li, D. Jiang, V. Bunpetch, Y. Hu, H. Ouyang, S. Zhang, Tough hydrogel with enhanced tissue integration and in situ forming capability for osteochondral defect repair, Appl. Mater. Today 13 (2018) 32–44.
[37] C.M. Madl, B.L. LeSavage, R.E. Dewi, C.B. Dinh, R.S. Stowers, M. Khariton, K.J. Lampe, D. Nguyen, O. Chaudhuri, A. Enejder, S.C. Heilshorn, Maintenance of neural progenitor cell stemness in 3D hydrogels requires matrix remodelling, Nat. Mater. 16 (2017) 1233–1242.
[38] C. Yu, J. Schimelman, P. Wang, K.L. Miller, X. Ma, S. You, J. Guan, B. Sun, W. Zhu, S. Chen, Photopolymerizable biomaterials and light-based 3D printing strategies for biomedical applications, Chem. Rev. 120 (2020) 10695–10743.
[39] A. Schwab, R. Levato, M. D'Este, S. Piluso, D. Eglin, J. Malda, Printability and shape fidelity of bioinks in 3D bioprinting, Chem. Rev. 120 (2020) 11028–11055.
[40] F. Zhou, Y. Hong, R. Liang, X. Zhang, Y. Liao, D. Jiang, J. Zhang, Z. Sheng, C. Xie, Z. Peng, X. Zhuang, V. Bunpetch, Y. Zou, W. Huang, Q. Zhang, E.V. Alakpa, S. Zhang, H. Ouyang, Rapid printing of bio-inspired 3D tissue constructs for skin regeneration, Biomaterials 258 (2020) 120287.
[41] Z. Belattmania, S. Kaidi, S. El Atouani, C. Katif, F. Bentiss, C. Jama, A. Reani, B. Sabour, V. Vasconcelos, Isolation and FTIR-ATR and $^{1}$H NMR characterization of alginates from the main alginophyte species of the atlantic coast of morocco, Molecules 25 (2020) 4335.
[42] F. Gao, Z. Xu, Q. Liang, H. Li, L. Peng, M. Wu, X. Zhao, X. Cui, C. Ruan, W. Liu, Osteochondral regeneration with 3D-printed biodegradable high-strength supramolecular polymer reinforced-gelatin hydrogel scaffolds, Adv. Sci. 6 (2019) 1900867.

[43] Y. Qiao, X. Liu, X. Zhou, H. Zhang, W. Zhang, W. Xiao, G. Pan, W. Cui, H.A. Santos, Q. Shi, Gelatin templated polypeptide Co-cross-linked hydrogel for bone regeneration, Adv. Healthc. Mater. 9 (2020) e1901239.
[44] Y. Yang, J. Zhang, Z. Liu, Q. Lin, X. Liu, C. Bao, Y. Wang, L. Zhu, Tissue-integratable and biocompatible photogelation by the imine crosslinking reaction, Adv. Mater. 28 (2016) 2724–2730.
[45] J.W. Nichol, S.T. Koshy, H. Bae, C.M. Hwang, S. Yamanlar, A. Khademhosseini, Cell-laden microengineered gelatin methacrylate hydrogels, Biomaterials 31 (2010) 5536–5544.
[46] K. Yue, G.T. Santiago, M.M. Alvarez, A. Tamayol, N. Annabi, A. Khademhosseini, Synthesis, properties, and biomedical applications of gelatin methacryloyl (GelMA) hydrogels, Biomaterials 73 (2015) 254–271.
[47] M.B. Browning, S.N. Cereceres, P.T. Luong, E.M. Cosgriff-Hernandez, Determination of the in vivo degradation mechanism of PEGDA hydrogels, J. Biomed. Mater. Res. A 102A (2014) 4244–4251.
[48] T. Pauloehrl, G. Delaittre, M. Bruns, M. Meissler, H.G. Borner, M. Bastmeyer, C. Barner-Kowollik, (Bio)molecular surface patterning by phototriggered oxime ligation, Angew. Chem. Int. Ed. 51 (2012) 9181–9184.
[49] J. Li, A.D. Celiz, J. Yang, Q. Yang, I. Wamala, W. Whyte, B.R. Seo, N.V. Vasilyev, J.J. Vlassak, Z. Suo, D.J. Mooney, Tough adhesives for diverse wet surfaces, Science 357 (2017) 378–381.
[50] Y. Zhang, C. Li, Q. Zhu, R. Liang, C. Xie, S. Zhang, Y. Hong, H. Ouyang, A long-term retaining molecular coating for corneal regeneration, Bioact. Mater. 6 (2021) 4447–4454.
[51] Q. Zhang, Q. Tang, Y. Yang, J. Yi, W. Wei, Y. Hong, X. Zhang, F. Zhou, X. Yao, H. Ouyang, Wound dressing gel with resisted bacterial penetration and enhanced re-epithelization for corneal epithelial-stromal regeneration, Appl. Mater. Today 24 (2021) 101119.
[52] K.Y. Lee, D.J. Mooney, Alginate: properties and biomedical applications, Prog. Polym. Sci. 37 (2012) 106–126.
[53] C.F. Labuschagne, E.C. Cheung, J. Blagih, M.C. Domart, K.H. Vousden, Cell clustering promotes a metabolic switch that supports metastatic colonization, Cell Metab 30 (2019) 720–734.
[54] Q. He, Y. Liao, J. Zhang, X. Yao, W. Zhou, Y. Hong, H. Ouyang, All-in-one" gel system for whole procedure of stem-cell amplification and tissue engineering, Small 16 (2020) e1906539.
[55] X. Long, X. Wang, L. Yao, S. Lin, J. Zhang, W. Weng, K. Cheng, H. Wang, J. Lin, Graphene/Si-promoted osteogenic differentiation of BMSCs through light illumination, ACS Appl. Mater. Interfaces 11 (2019) 43857–43864.
[56] Q. Meng, J. Gao, H. Zhu, H. He, Z. Lu, M. Hong, H. Zhou, The proteomic study of serially passaged human skin fibroblast cells uncovers down-regulation of the chromosome condensin complex proteins involved in replicative senescence, Biochem. Bioph. Res. Co. 505 (2018) 1112–1120.
[57] M.J. Dalby, N. Gadegaard, R.O.C. Oreffo, Harnessing nanotopography and integrin–matrix interactions to influence stem cell fate, Nat. Mater. 13 (2014) 558–569.
[58] D. Seliktar, Designing cell-compatible hydrogels for biomedical applications, Science 336 (2012) 1124–1128.
[59] Y.N. Zhang, R.K. Avery, Q. Vallmajo-Martin, A. Assmann, A. Vegh, A. Memic, B.D. Olsen, N. Annabi, A. Khademhosseini, A highly elastic and rapidly crosslinkable elastin-like polypeptide-based hydrogel for biomedical applications, Adv. Funct. Mater. 25 (2015) 4814–4826.
[60] C. Hrabchak, J. Rouleau, I. Moss, K. Woodhouse, M. Akens, C. Bellingham, F. Keeley, M. Dennis, A. Yee, Assessment of biocompatibility and initial evaluation of genipin cross-linked elastin-like polypeptides in the treatment of an osteochondral knee defect in rabbits, Acta Biomater 6 (2010) 2108–2115.
[61] S. Abbasi, S. Sinha, E. Labit, N.L. Rosin, G. Yoon, W. Rahmani, A. Jaffer, N. Sharma, A. Hagner, P. Shah, R. Arora, J. Yoon, A. Islam, A. Uchida, C.K. Chang, J.A. Stratton, R.W. Scott, F.M.V. Rossi, T.M. Underhill, J. Biernaskie, Distinct regulatory programs control the latent regenerative potential of dermal fibroblasts during wound healing, Cell Stem Cell 27 (2020) 396–412.
[62] M. Ito, Y. Liu, Z. Yang, J. Nguyen, F. Liang, R.J. Morris, G. Cotsarelis, Stem cells in the hair follicle bulge contribute to wound repair but not to homeostasis of the epidermis, Nat. Med. 11 (2005) 1351–1354.
[63] P. Mostafalu, G. Kiaee, G. Giatsidis, A. Khalilpour, M. Nabavinia, M.R. Dokmeci, S. Sonkusale, D.P. Orgill, A. Tamayol, A. Khademhosseini, A textile dressing for temporal and dosage controlled drug delivery, Adv. Funct. Mater. 27 (2017) 1702399.
[64] A.M. Vignola, J. Kips, J. Bousquet, Tissue remodeling as a feature of persistent asthma, J. Allergy. Clin. Immunol. 105 (2000) 1041–1053.
[65] J. Qu, X. Zhao, Y. Liang, T. Zhang, P.X. Ma, B. Guo, Antibacterial adhesive injectable hydrogels with rapid self-healing, extensibility and compressibility as wound dressing for joints skin wound healing, Biomaterials 183 (2018) 185–199.
[66] L.A. DiPietro, Angiogenesis and scar formation in healing wounds, Curr. Opin. Rheumatol. 25 (2013) 87–91.
[67] Z. Wu, Y. Hong, Combination of the silver-ethylene interaction and 3D printing to develop antibacterial superporous hydrogels for wound management, ACS Appl. Mater. Interfaces 11 (2019) 33734–33747.
[68] Y. Yang, Y. Liang, J. Chen, X. Duan, B. Guo, Mussel-inspired adhesive antioxidant antibacterial hemostatic composite hydrogel wound dressing via photo-polymerization for infected skin wound healing, Bioact. Mater. 8 (2022) 341–354.
[69] X. Wang, J. Qi, W. Zhang, Y. Pu, R. Yang, P. Wang, S. Liu, X. Tan, B. Chi, 3D-printed antioxidant antibacterial carboxymethyl cellulose/epsilon-polylysine hydrogel promoted skin wound repair, Int. J. Biol. Macromol. 187 (2021) 91–104.